Applied Surface Science 311 (2014) 369–376

Contents lists available at ScienceDirect

Applied Surface Science

journal homepage: www.elsevier.com/locate/apsusc

Characterizations of nano-TiO_2/diatomite composites and their photocatalytic reduction of aqueous Cr (VI)

Qing Sun, Hui Li, Shuilin Zheng*, Zhiming Sun**

School of Chemical and Environmental Engineering, China University of Mining and Technology (Beijing), Beijing 100083, PR China

ARTICLE INFO

Article history:
Received 20 February 2014
Received in revised form 15 April 2014
Accepted 12 May 2014
Available online 19 May 2014

Keywords:
Photocatalysis
Cr (VI)
TiO_2
Diatomite

ABSTRACT

In this paper, the TiO_2 nanoparticles were immobilized on diatomite (DIA) via a typical hydrolysis precipitation process using $TiCl_4$ as precursor. The as-prepared composites were characterized by X-ray diffraction (XRD), scanning electron microscopy (SEM), transmission electron microscopy (TEM) and X-ray photoelectron spectroscopy (XPS). TiO_2 nanoparticles with the average grain size of around 7–14 nm were well deposited on the surface of diatomite. The photocatalytic activity toward the reduction of aqueous Cr (VI) was demonstrated under UV light. The influence of initial pH values, catalyst amount, illumination intensity and initial concentration of Cr (VI) on photocatalytic reduction of Cr (VI) were investigated. Compared with the commercial TiO_2 (P25, Degussa), the TiO_2/DIA composites had better reactive activity because of their relatively higher adsorption capacity. Furthermore, the prepared photocatalyst exhibited relatively good photocatalytic stability depending on the reusability tests.

1. Introduction

Nowadays, heavy metals, such as cadmium, zinc, copper, lead, mercury, nickel and chromium, have been excessively released into environment because of the rapid industrialization [1]. Cr (VI) is a highly toxic pollutant causing carcinogenic, mutagenic and teratogenic effects on specific organisms. And the maximum concentration authorized in drinking water in China is restricted at 0.05 mg/L. In contrast, Cr (III) has much less toxicity than that of Cr (VI) and can be easily precipitated as $Cr(OH)_3$ in neutral or alkaline solutions [2]. However, the deficiencies of high cost or secondary pollution exist in the traditional chemical or biological degradation methods [3,4]. Hence, it is highly desirable to explore an economical and efficient technique for the reduction of Cr (VI).

Titanium dioxide has been widely used as a photocatalytic material due to its photocatalytic stability, low cost and nontoxicity [5]. It has been proved that most of the organic pollutants, such as phenol, formaldehyde, dyes and pesticides, can be mineralized by TiO_2 [6–8]. Numerous previous literatures have proved that toxic Cr (VI) can be reduced to a less harmful state Cr (III) through the photocatalytic reduction by pure TiO_2 nanoparticles [9,10]. However, pure TiO_2 nanoparticles are easy to agglomerate and difficult to be separated and recycled in practical applications. Natural porous minerals with a high surface area and strong adsorption ability can be used as the supports to load the TiO_2 nanoparticles. In recent years, a number of studies have showed that the combination of TiO_2 with these materials not only solved the TiO_2 nanoparticles agglomeration problem, but also improved the photocatalytic performance of pure TiO_2 [11–14]. Due to its unique microporous structure, high specific surface area, strong sorption ability and chemical stability, diatomite (DIA) has been widely used as a natural adsorbent for heavy metals removal in water purification [15–17].

In the present work, nano-TiO_2/DIA composites are synthesized through a typical hydrolysis precipitation process using $TiCl_4$ as precursor. The compositions, structure, and morphology of the obtained products were characterized by XRD, SEM, TEM and XPS. The photocatalytic reactivity was investigated by the reduction of aqueous Cr (VI) as a target pollutant. Besides, the reusability tests were performed in order to determine the photocatalytic stability of the prepared catalysts.

2. Experimental

2.1. Preparation of DIA-supported TiO_2

DIA used in this study was collected from Linjiang (Jilin province, China) and acid leached to remove impurities. Stock solution (100 mg/L) of Cr (VI) was prepared by dissolving analytic grade

* Corresponding author. Fax: +86 10 62330972.
** Corresponding author. Fax: +86 10 82375166.
E-mail addresses: shuilinzh@sina.com (S. Zheng), szmcumtb@hotmail.com (Z. Sun).

http://dx.doi.org/10.1016/j.apsusc.2014.05.070
0169-4332/

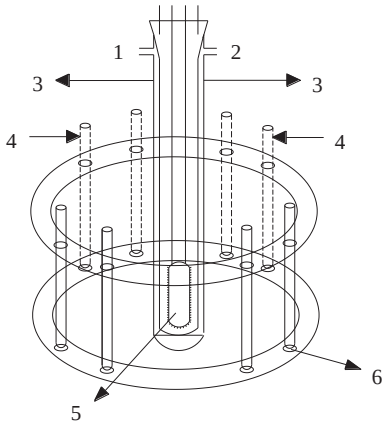

Fig. 1. Schematic diagram of photocatalysis reactor (1: cooling water entrance, 2: cooling water outlet, 3: quartz tube, 4: quartz reactor, 5: UV lamp, 6: magnetic stirrer).

$K_2Cr_2O_7$ (Beijing Chemical Reagent Plant) into distilled water. Experimental solutions of the desired concentration were obtained by successive dilutions. For comparison, pure commercial TiO_2 (P25, Degussa AG, Germany) particles were also used as reference. The other reagents were of analytical grade and distilled water was used in this experiment. A description of the synthesis the nano-TiO_2/diatomite composite by a hydrolysis precipitation process has been reported previously [18]. Briefly, diatomite was mixed with distilled water in a stirring ice-water bath. Meanwhile, HCl was added into the suspension. Then, a certain amount of $(NH_4)_2SO_4$ and $TiCl_4$ were dropped slowly into the mixture. $NH_3{\cdot}H_2O$ was used to adjust pH value for the hydrolysis precipitation reaction. The final powders were washed free of chloride anions as determined by $AgNO_3$ (0.1 mol/L), dried in an oven at 105 °C for 10 h. Finally, the TiO_2 particles immobilized on DIA were crystallized through calcinations at different temperatures for 2 h. For comparison, pure TiO_2 powder was also prepared by the same procedure without the addition of DIA.

2.2. Photocatalytic reactor and experimental procedure

A water-jacket system equipped with a high-pressure UV lamp was used in the photocatalytic reaction. There were eight 150 mL cylindrical quartz reactors around the cylindrical-quartz tube as shown in Fig. 1. The pH of Cr (VI) reaction solution for each experiment was adjusted together in order to maintain the same pH values of Cr (VI) solution in eight containers. 1000 mL of Cr (VI) working solution was diluted from stock solution (100 mg/L) of Cr (VI) before each experiment and the solution pH was adjusted by dilute HCl or NaOH and monitored by a pH meter (FE20, Mettler-Toledo Instruments Co., Ltd) during the dilution process. The catalysts and 100 mL of Cr (VI) reaction solution were added into each of eight cylindrical quartz reactors and stirred by a magnetic stirrer. Absorption experiments were carried out in dark with catalyst. Blank tests were investigated by the same procedure, but without the addition of catalyst. After a period of reaction, one of the eight cylindrical quartz reactors was moved out periodically and 5 mL of the suspensions were centrifuged (TDL-5-A, Shanghai Anting Co., Ltd) and filtered with a 0.45 μm membrane filter to remove sample particles and then 2 mL of dissolved Cr (VI) solution was collected and analyzed individually. The membrane filter has no absorption for Cr (VI) according to the previous literatures [19–21]. The concentration of Cr (VI) was determined by diphenylcarbazide (DPC) colorimetric method at 540 nm and the detection limit is 5 μg/L [22–25].

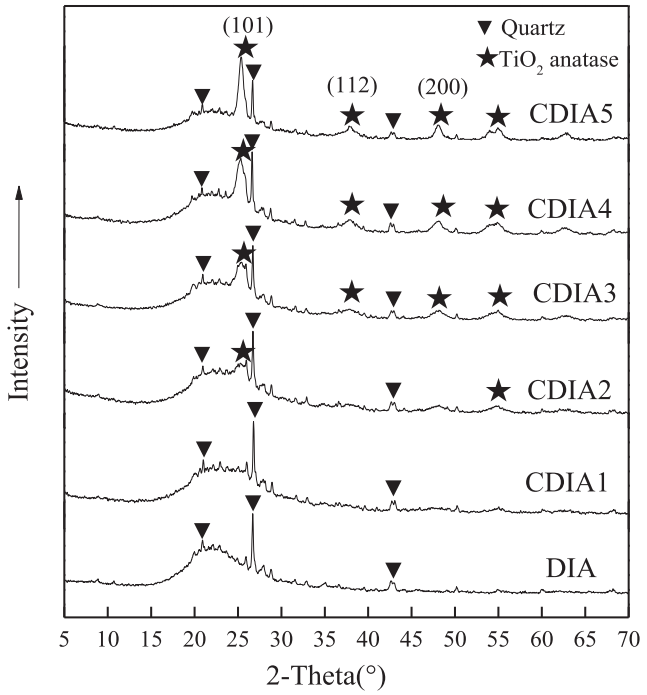

Fig. 2. XRD patterns of the samples: DIA powder; nano-TiO_2/DIA composites power calcined at 300 °C (CDIA1), 400 °C (CDIA2), 500 °C (CDIA3), 600 °C (CDIA4), 700 °C (CDIA5), respectively.

2.3. Analysis and characterizations

The structure of the samples was characterized by X-ray diffraction (XRD, Rigaku D/max 2500) using Cu-Kα radiation (λ = 1.54178 Å). The morphology of samples was measured by scanning electron microscopy (SEM, S-4800 Hitachi, Japan). The transmission electron microscopy (TEM) measurements were carried out on a JEM-1200EX (JEOL, Japan) electron microscope operating at an acceleration voltage of 120 kV. The specific surface area and pore size distribution of samples were measured by a BET nitrogen adsorption–desorption isotherm measurement (BET, JW-BK, Jingwei). Element state in the samples was measured by X-ray photo spectrometer (XPS, ESCALAB 250Xi, Thermo Scientific) using Mg-Kα radiation (1253.6 eV). The binding energy calibration was performed using C1s peak as a reference.

3. Results and discussion

3.1. Characterizations of samples

The crystal phase of DIA and nano-TiO_2/DIA composites calcined at different temperatures is shown in Fig. 2. The XRD pattern of DIA was well in agreement with that of the characteristic amorphous SiO_2. No peaks of other impurities but only the quartz were observed and the purity of DIA was high. As for nano-TiO_2/DIA composites, the peaks corresponding to anatase TiO_2 were observed except for that of quartz and amorphous SiO_2. The sample calcined at 300 °C was composed of amorphous phase of anatase. With increasing the calcination temperature, the degree of TiO_2 crystallization in composites was improved gradually. Based on the XRD results, the crystal size of the TiO_2 was determined according to the Scherrer equation [26], and the calculated results were summarized in Table 1.

The calcination is an important means to promote the transformation of amorphous to crystalline and adjust the grain sizes [27]. From Table 1, the crystal size of TiO_2 in samples was increased from

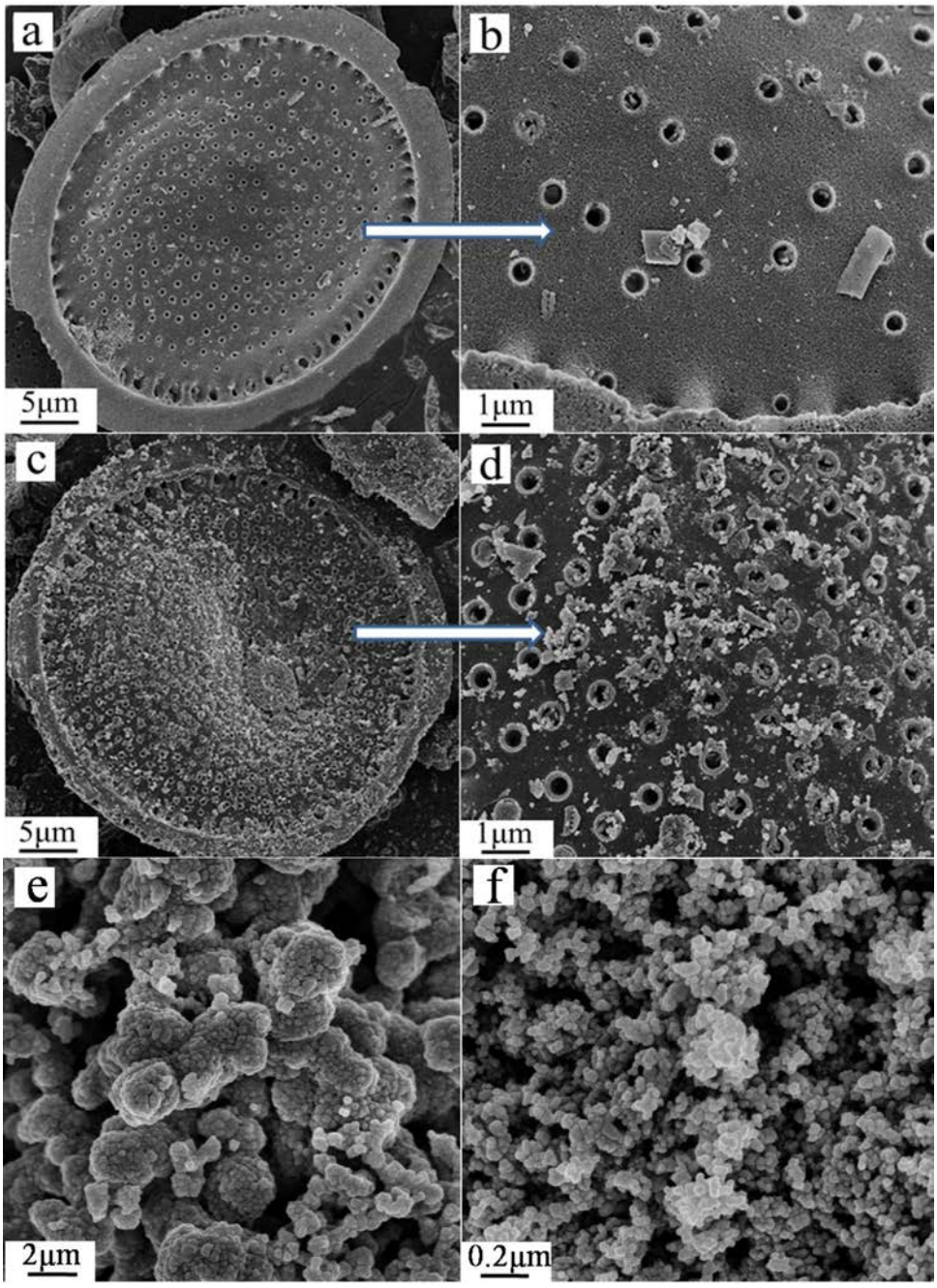

Fig. 3. SEM micrograph of DIA (a and b), CDIA5 (c and d), pure TiO_2 (e) and P25 (f).

7.43 nm to 13.08 nm with the calcination temperature increasing from 400 °C to 700 °C. According to the previous literature, TiO_2 of larger crystal size and higher anatase content exhibits a relatively higher catalytic efficiency [28]. Therefore, 700 °C was chosen as the optimum calcinations condition.

Table 1
Crystal parameters and grain size for nano-TiO_2/DIA composites calcined at different temperatures.

Sample	Temperature (°C)	2θ (°)	$B_{(101)}$, TiO_2	$D_{(101)}$ (nm)
CDIA1	300	–	–	–
CDIA2	400	25.346	0.018919	7.43
CDIA3	500	25.386	0.017087	8.23
CDIA4	600	25.327	0.014608	9.63
CDIA5	700	25.363	0.010751	13.08

Fig. 3 presents the SEM micrographs of DIA (Fig. 3a and b), CDIA5 (Fig. 3c and d), pure TiO_2 (Fig. 3e) and P25 (Fig. 3f). As can be observed from Fig. 3a and b, the DIA possesses a disk-like shape and highly ordered porous structure. As shown in Fig. 3c and d, some micro-aggregate particles appear on the surface of the composites due to the introduction of the TiO_2 particles. Serious agglomeration of the particles was found from the SEM images of pure TiO_2 and P25. Compared with pure TiO_2, it can be seen that the distribution of TiO_2 nanoparticles are relatively uniform. The chemical and BET analysis results of samples before and after loading of TiO_2 are summarized in Table 2. The content of TiO_2 in CDIA5 is up to 15.02 wt%. And the BET surface area of the composite materials increases after TiO_2 deposition. However, the pore size decreases because of the immobilization of the TiO_2 particles on DIA.

Table 2
Chemical compositions and physical structural data of DIA and CDIA5.

	DIA	CDIA5
Chemical compositions (wt%)	Main: SiO_2, 91.36; TiO_2, 0.20; Fe_2O_3, 0.32; CaO, 0.30	Main: SiO_2, 81.46; TiO_2, 15.02; Fe_2O_3, 0.12; CaO, 0.31
BET surface area (m^2/g)	20.88	29.70
Pore size (nm)	8.85	8.06

Fig. 4 shows the XPS survey spectra of DIA (a) and CDIA5 (b). The characteristic peaks for O, Si and C can be observed from Fig. 4(a). Compared with the XPS survey spectrum of DIA, the characteristic peaks for Ti were also observed in composite materials, which further confirmed the existence of TiO_2 in the sample. The photoelectron peaks for Ti2p, O1s, Si2p and C1s were located at binding energies of 458.3 eV, 532.7 eV, 103.6 eV and 284.8 eV, respectively [29,30]. No obvious shift of binding energy of Si2p was observed after the introduction of the TiO_2 particles according to Fig. 5A. It is concluded that the immobilization of TiO_2 on DIA may be a physical precipitation and adsorption process. The O1s spectrum of CDIA5 displayed two distinct peaks as shown in Fig. 5B(b). The higher peak of the binding energy at 532.8 eV is related to the hydroxyl group. The other peak at 529.8 eV is attributed to Ti—O in TiO_2 [31]. As displayed in Fig. 5C(b), the binding energies of Ti($2p_{3/2}$) and Ti($2p_{1/2}$) exhibit two peaks centered at 458.3 eV and 464.3 eV, respectively, suggesting the existence of pure anatase TiO_2 in composite material [32].

TEM images of pure TiO_2 powder (a) and CDIA5 (b) are shown in Fig. 6. From Fig. 6a, the particle size of pure TiO_2 powder is around 20–50 nm. The TiO_2 nanoparticles without carrier tend to aggregate together due to the strong physical interaction. From Fig. 6b, the TiO_2 nanoparticles distributed on the surface or in the pores of DIA. Only a small number of fine particles accumulate together loosely. Hence, DIA as the catalyst carrier also plays a dispersant role in the preparation of the composite catalysts.

3.2. *Effect of pH on the Cr (VI) degradation*

The solution pH plays an important role in the reduction of Cr (VI). To determine the optimum pH, a batch of experiments has been performed by varying the pH in the range of 1–10 on the absorption and reduction of Cr (VI). The influence of pH on the adsorption and reduction of Cr (VI) on the CDIA5 is presented in Fig. 7.

As shown in Fig. 7, it can be seen that the adsorption and photocatalytic efficiency decreased gradually with changing the initial

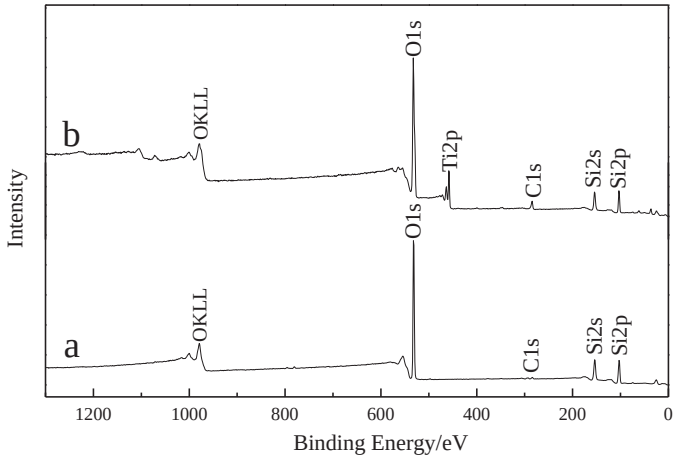

Fig. 4. XPS survey scan spectrum of DIA (a) and CDIA5 (b).

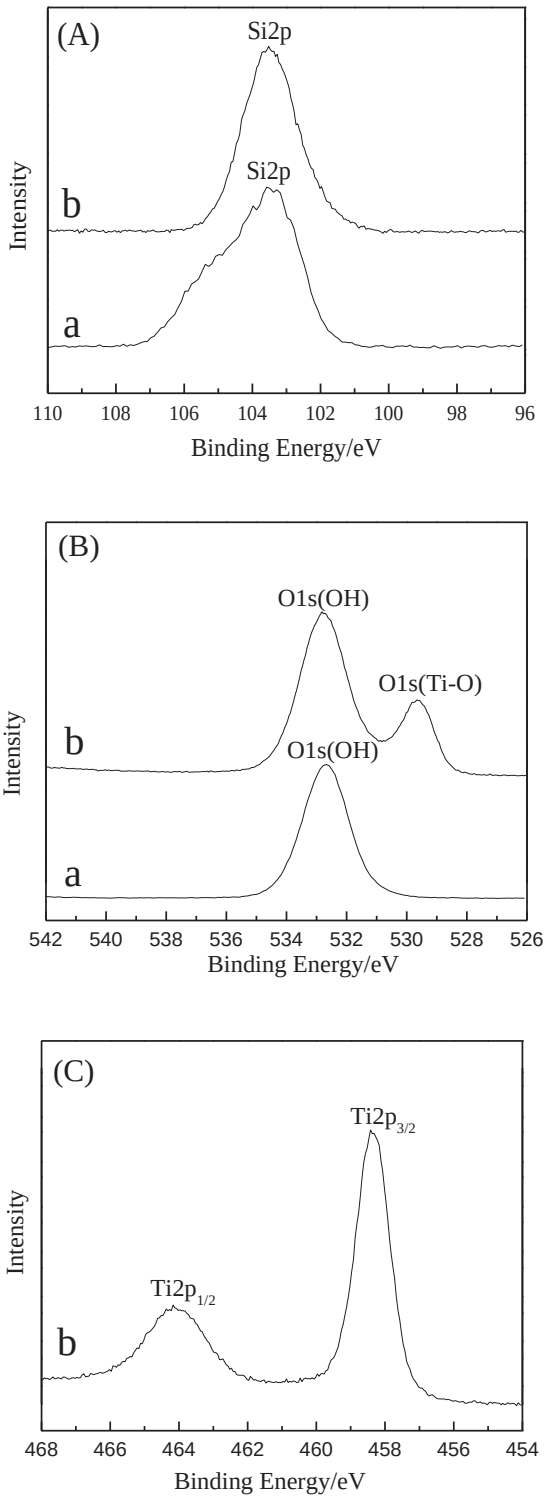

Fig. 5. High resolution XPS spectra of Si2p (A), O1s (B) and Ti2p(C) peaks of DIA (a) and CDIA5 (b).

pH from 2 to 10. The optimum pH is 2.1 and the removal efficiency is up to 57.83%. The photocatalytic reduction rate of Cr (VI) started to decline when pH < 2. According to the previous literatures, the relevant reactions during the reduction of Cr (VI) by TiO_2 can be expressed as follows [33,34]:

$$TiO_2 \xrightarrow{h\nu} e^- + h^+ \quad (1)$$

$$Cr_2O_7^{2-} + 14H^+ + 6e^- \rightarrow 2Cr^{3+} + 7H_2O \quad (2)$$

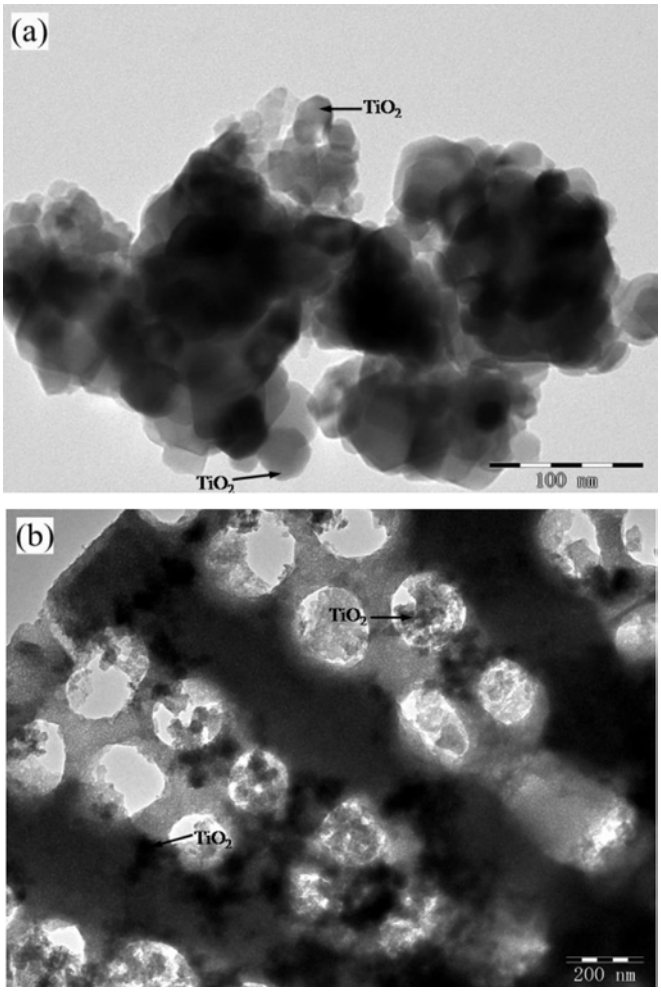

Fig. 6. TEM micrographs of pure TiO_2 (a) and CDIA5 (b).

$$2H_2O + 4h^+ \rightarrow O_2 + 4H^+ \quad (3)$$

Under UV light, the electron and hole pairs generate in the surface of TiO_2 as shown in the Eq. (1). From Eq. (2), the greater the concentration of H^+ in solution is, the higher the degradation efficiency of Cr (VI) is. Hence, the photocatalytic reduction of Cr (VI) can be enhanced at acid condition. However, excessive H^+ might inhibit the Eq. (3) causing the decrease of the reduction efficiency of Cr (VI).

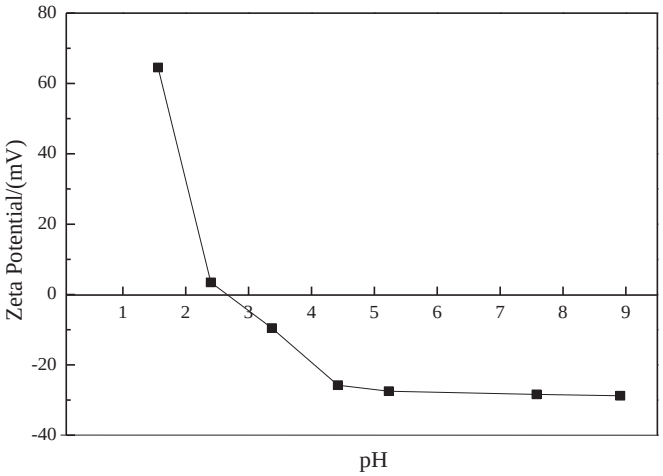

Fig. 8. Effect of initial pH on the zeta potential of CDIA5.

Fig. 8 displays the change of zeta potential of CDIA5 at different pH values. From Fig. 8, the pH_{zpc} (pH of zero point charge) of CDIA5 is 2.66. When pH < 2.66, the surface of composite is electropositive, which is in favor of the adsorption of the Cr (VI) anions ($Cr_2O_7^{2-}$). The improvement of the adsorption can promote photocatalytic reduction efficiency of Cr (VI) [35]. On the contrary, the surface of catalyst becomes electronegative when pH > 2.66, and the adsorption capacity for Cr (VI) anions decreases, which is in line with the previous experimental results. It is concluded that the adsorption capacity for Cr (VI) anions of samples played an important role in the photocatalytic reaction.

3.3. *Effect of the amount of samples*

The effect of the catalysts amount on the photocatalytic reduction rate of Cr (VI) is displayed in Fig. 9. A blank test without catalysts was also carried out as reference. The catalysts amount

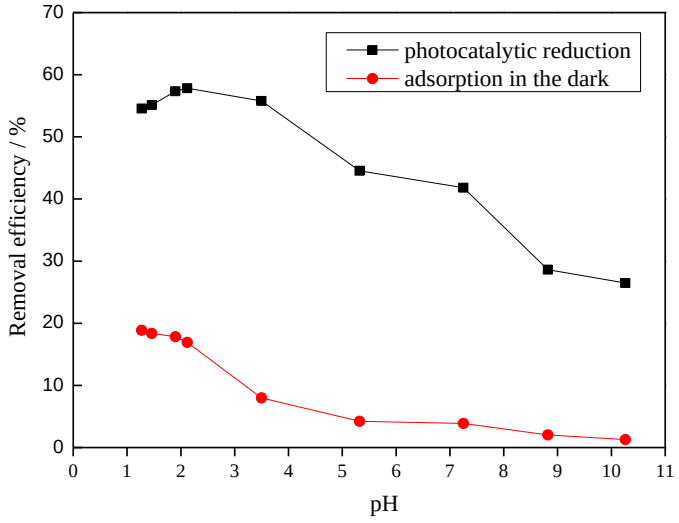

Fig. 7. Influence of initial pH on the Cr (VI) removal effect (experimental conditions: initial [Cr (VI)] = 10 mg/L, catalyst amount = 2 g/L, reaction time = 180 min, adsorption in dark and UV light = 300 W, respectively).

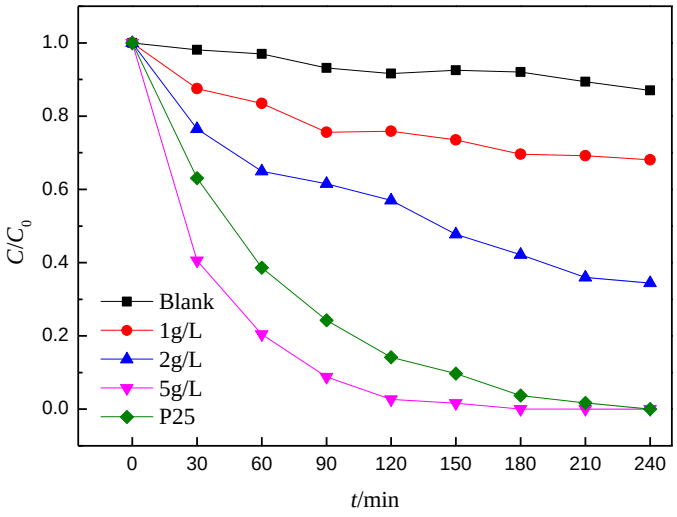

Fig. 9. Influence of catalysts amount on the removal effect of Cr (VI) (experimental conditions: [Cr (VI)] = 10 mg/L, UV light intensity = 300 W, pH = 2.1).

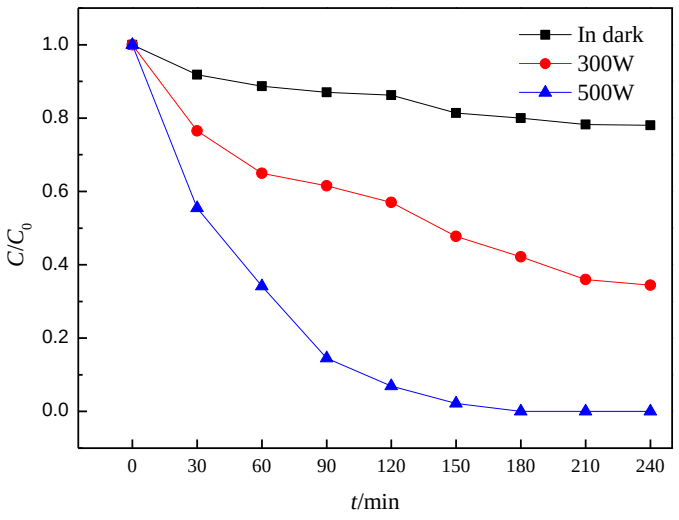

Fig. 10. Influence of the illumination intensity and on the removal effect of Cr (VI) (experimental conditions: catalyst amount = 2 g/L, [Cr (VI)] = 10 mg/L, pH = 2.1).

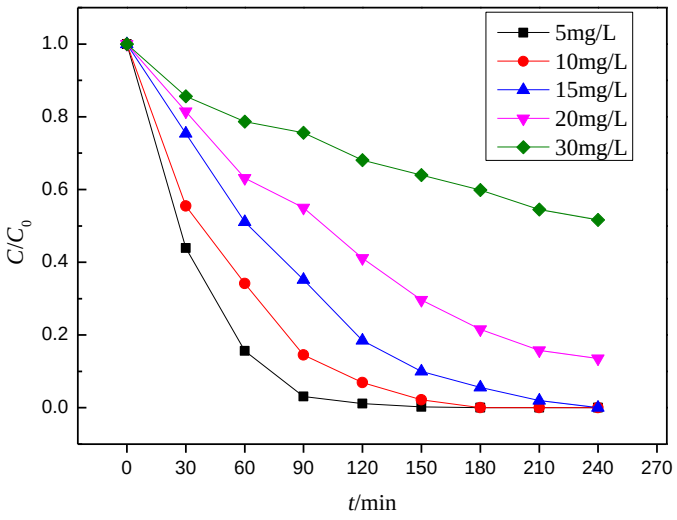

Fig. 11. Influence of initial Cr (VI) concentration on the removal effect of Cr (VI) (experimental conditions: catalyst amount = 2 g/L, UV light intensity = 500 W, pH = 2.1).

of P25 sample was 0.75 g/L, which is equal with the TiO_2 content of 5 g/L of CDIA5.

As described in Fig. 9, the removal rate of Cr (VI) under UV light is unsatisfactory under low catalysts amount, which is in agreement with the previous results [36,37]. With increasing the catalysts amount, the reduction rate of Cr (VI) increases gradually. The increase of the catalysts amount provides more photocatalytic reactive sites for the reduction of Cr (VI). The reduction rate is up to about 100% within 150 min when the catalyst amount is 5 g/L. On the other hand, the commercial TiO_2 (P25) possesses a lower removal efficiency compared with CDIA5 under the same catalyst (TiO_2) amount. According to the previous adsorption tests, it is suggested that the CDIA5 sample exhibited a better photocatalytic activity for Cr (VI) due to its higher adsorption capacity.

3.4. Effect of the illumination intensity

Fig. 10 shows the Cr (VI) reduction by CDIA5 composite when intensity of UV illumination is varied from 0 to 500 W. It is evident that the maximum adsorption removal rate of Cr (VI) is less than 20% in dark within 150 min. The photocatalytic reduction of Cr (VI) is significantly improved under UV light. It is also observed that the removal rate of Cr (VI) increases with increasing the illumination intensity. It is attributed to the fact that more electron–hole pairs are generated under higher illumination intensity. Therefore, more electrons will be available for the photocatalytic reduction of Cr (VI). The removal rate of Cr (VI) reaches almost 98% within 150 min under the illumination intensity of 500 W.

3.5. Effect of Cr (VI) concentration

Fig. 11 displays the influence of initial Cr (VI) concentration varying from 5 mg/L to 30 mg/L on the degradation effect of catalysts. It is indicated that the Cr (VI) removal efficiency strongly depends on the initial Cr (VI) concentration. With increasing the Cr (VI) concentration, the removal rate of Cr (VI) gradually decreases. On the other hand, the reaction rate becomes slower under higher concentration.

From Fig. 11, almost 100% Cr (VI) in solution has been reduced to Cr (III) at concentration of 5 mg/L, 10 mg/L and 15 mg/L under the UV illumination within 240 min. To identify the absorption and reduction of chromium in catalyst after the photocatalytic reaction, the dry CDIA5 sample after Cr (VI) degradation was adopted to XPS analysis. High resolution XPS spectra of Cr peaks are shown in Fig. 12. The bands at binding energy of 577.2 eV, 580.6 eV and 585.9 eV are attributed to Cr (III) $2p_{3/2}$, Cr (VI) $2p_{3/2}$ and Cr (III) $2p_{1/2}$, respectively [38–41]. The total Cr concentration in the sample determined by XPS is 0.13 at%. Based on the corresponding peak area, the proportion of Cr (III) and Cr (VI) are 55.6% and 44.4%, respectively [42]. The result confirms that the adsorption and reduction of Cr (VI) occurred simultaneously under the UV illumination.

3.6. Kinetic modeling

It has been reported that heterogeneous photocatalytic reaction follows the Langmuir–Hinshelwood (L–H) kinetic model [43–45], which can be expressed as the following equation:

$$r_0 = -\frac{dC}{dt} = \frac{kKC_0}{1 + KC_0} \quad (4)$$

where r_0 is the initial photocatalytic degradation efficiency (mg/(L min)); k is the apparent reaction efficiency constant (mg/(L min)); and K is the reaction equilibrium constant (L/mg).

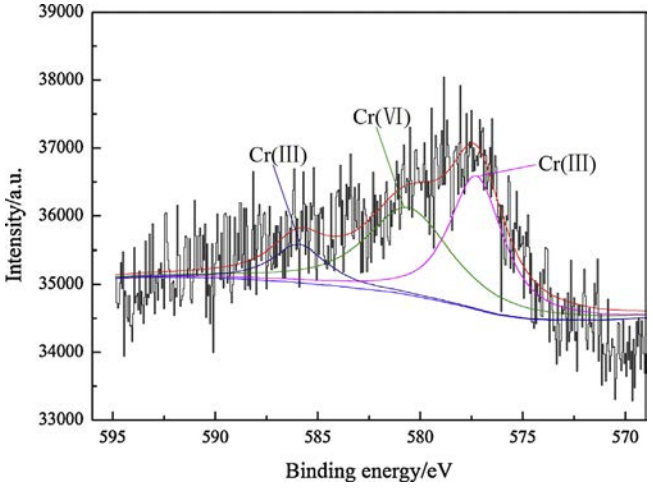

Fig. 12. High resolution XPS spectrum of Cr on the surface of CDIA5 catalyst (experimental conditions: catalyst amount = 2 g/L, UV light intensity = 500 W, pH = 2.1, reaction time = 240 min).

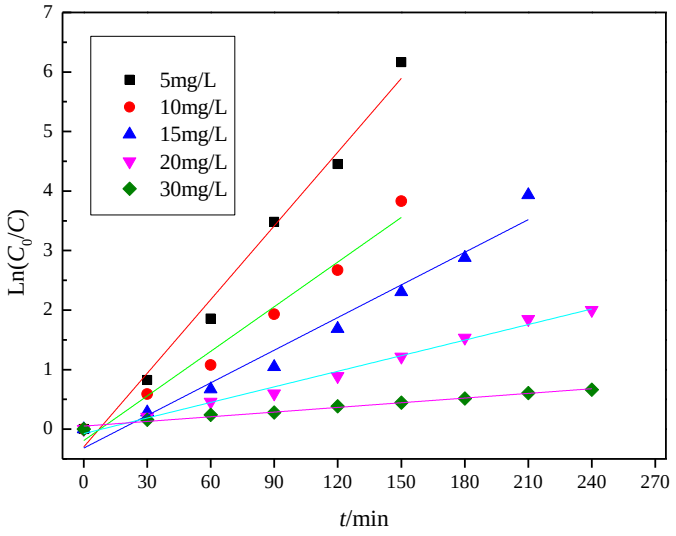

Fig. 13. The photocatalytic reduction of Cr (VI) kinetics curve in different initial concentration.

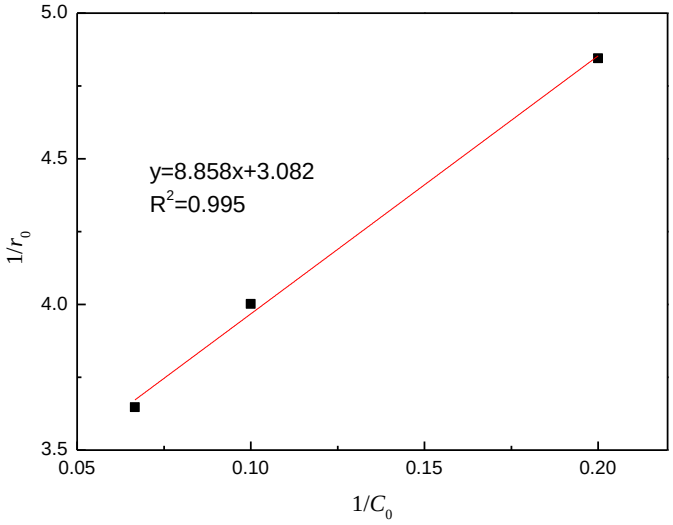

Fig. 14. The fitted curve between $1/r_0$ and $1/C_0$ at initial the concentrations 5 mg/L, 10 mg/L and 15 mg/L.

When the solution is highly diluted into a millimolar solution, the denominator of Eq. (4) is neglected and the equation can be simplified to an apparent first order equation [46,47]:

$$r_0 = -\frac{dC}{dt} = kKC_0 = k_{ap}C_0 \quad (5)$$

where k_{ap} is the apparent rate constant of a pseudo first order reaction. So Eq. (5) can be transformed to a first order equation:

$$\ln\left(\frac{C_0}{C}\right) = k_{ap}t \quad (6)$$

The plot $\ln(C_0/C)$ versus t for the concentrations 5 mg/L,10 mg/L, 15 mg/L, 20 mg/L and 30 mg/L describes a linear behavior as described in Fig. 13. The correlation coefficients (R^2) indicate that the photocatalytic reduction of Cr (VI) follows the pseudo first order reaction. The slope of the linear regression equals the apparent first-order rate constant k_{ap} and the calculated parameters are summarized in Table 3.

The Eq. (4) can be rearranged into linear form:

$$\frac{1}{r_0} = \frac{1}{kKC_0} + \frac{1}{k} \quad (7)$$

The linearization of the curve in Fig. 14, plotting $1/r_0$ versus $1/C_0$, from 5 mg/L to 15 mg/L of initial concentration of the Cr (VI) describes a linear behavior with correlation coefficient $R^2 = 0.995$. It is indicated that the photocatalytic reduction of Cr (VI) by CDIA5 fitted well with the L–H kinetic model.

3.7. Photocatalytic stability

It is important to investigate the reusability of the as-synthesized catalyst in order to evaluate the photocatalytic performance. Therefore, the CDIA5 was recycled for 4 times in the same photocatalytic reaction. After each reuse cycle, the photocatalyst was separated from the suspension by filtration and dried at 105 °C for 10 h. The photocatalytic performance of the CDIA5 in the four reuse cycles was displayed in Fig. 15. Obviously, the photocatalytic reduction efficiency of Cr (VI) decreases gradually with the increase in the number of reuse cycles. This should result from the decrease of adsorption and active sites on the surface of CDIA5 because of the deposition of $Cr(OH)_3$ generated after photocatalytic reactions. However, the removal efficiency of CDIA5 is still greater that 50% after four consecutive recycle uses, which indicates that the composites are stable photocatalysts for repeated usage.

Table 3
The relevant parameters obtained from kinetic study.

C_0 (mg/L)	k_{ap} (min^{-1})	r_0 (mg/(L min))
5	0.04128	0.2064
10	0.02499	0.2499
15	0.01828	0.2742
20	0.00872	0.1744
30	0.00262	0.0786

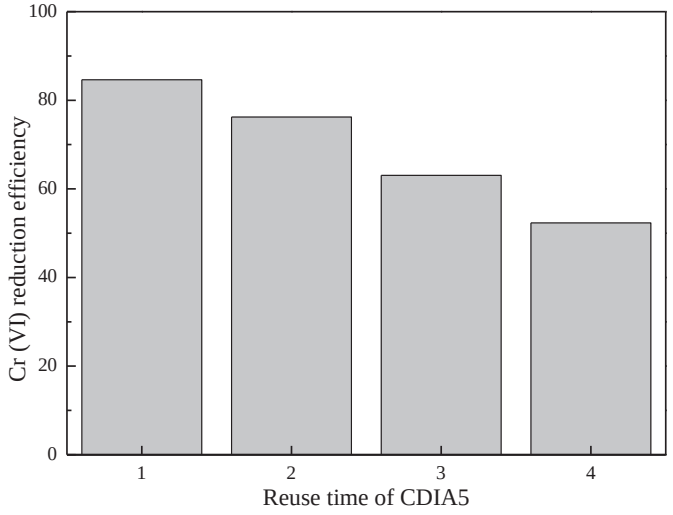

Fig. 15. Influence of reuse of catalyst on the removal of Cr (VI) (experimental conditions: catalyst amount = 2 g/L, UV light = 500 W, pH 2.1, [Cr (VI)] = 10 mg/L).

4. Conclusions

TiO_2 nanoparticles were immobilized on DIA by a typical hydrolysis precipitation process and the prepared nano-TiO_2/DIA composites were characterized by XRD, SEM, TEM and XPS. The TiO_2 nanoparticles are successfully immobilized on the surface of DIA in the crystal of anatase and the average grain size of nano-TiO_2 is 13.08 nm when the calcination temperature is 700 °C. Cr (VI) in solution can be effectively reduced by nano-TiO_2/DIA composites under UV illumination. The reduction efficiency of Cr (VI) increases

with increasing the amount of samples, increasing the illumination intensity and decreasing initial concentrations of Cr (VI). The photocatalytic reduction rate of Cr (VI) is up to 100% within 150 min under the illumination intensity of 300 W. The composites have a better activity than the commercial TiO_2 (P25) because of dispersive effect and high adsorption capacity of DIA. The removal kinetics for the reduction of Cr (VI) fit well with the Langmuir–Hinshelwood kinetic model within the Cr (VI) concentrations range of 5–15 mg/L. The reusability tests of catalyst indicate that the composites are stable photocatalysts for repeated usage.

Acknowledgment

The authors gratefully acknowledge financial support by the National Technology R&D Program in the 12th five years plan of China (2011BAB03B07).

References

[1] D. Damodaran, K. Vidya Shetty, B. Raj Mohan, Effect of chelaters on bioaccumulation of Cd (II), Cu (II), Cr (VI), Pb (II) and Zn (II) in *Galerina vittiformis* from soil, Int. Biodeterioration Biodegrad. 85 (2013) 182–188.
[2] M. Kebir, M. Chabani, N. Nasrallah, A. Bensmaili, M. Trari, Coupling adsorption with photocatalysis process for the Cr (VI) removal, Desalination 270 (2011) 166–173.
[3] C.E. Barrera-Díaz, V. Lugo-Lugo, B. Bilyeu, A review of chemical, electrochemical and biological methods for aqueous Cr (VI) reduction, J. Hazard. Mater. 223–224 (2012) 1–12.
[4] F. Pagnanelli, C. Cruz Viggi, A. Cibati, D. Uccelletti, L. Toro, C. Palleschi, Biotreatment of Cr (VI) contaminated waters by sulphate reducing bacteria fed with ethanol, J. Hazard. Mater. 199–200 (2012) 186–192.
[5] Y. Liao, C. Xie, Y. Liu, H. Chen, H. Li, J. Wu, Comparison on photocatalytic degradation of gaseous formaldehyde by TiO_2, ZnO and their composite, Ceram. Int. 38 (2012) 4437–4444.
[6] G. Zhang, X. Qin, Efficient photocatalytic degradation of gaseous formaldehyde by the TiO_2/tourmaline composites, Mater. Res. Bull. 48 (2013) 3743–3749.
[7] Z. Sun, C. Bai, S. Zheng, X. Yang, R.L. Frost, A comparative study of different porous amorphous silica minerals supported TiO_2 catalysts, Appl. Catal. A: Gen. 458 (2013) 103–110.
[8] S.H. Lin, C.H. Chiou, C.K. Chang, R.S. Juang, Photocatalytic degradation of phenol on different phases of TiO_2 particles in aqueous suspensions under UV irradiation, J. Environ. Manage. 92 (2011) 3098–3104.
[9] X. Chen, S.S. Mao, Titanium dioxide nanomaterials: synthesis, properties, modifications, and applications, Chem. Rev. 107 (2007) 2891–2959.
[10] S.G. Schrank, H.J. José, R.F.P.M. Moreira, Simultaneous photocatalytic Cr(VI) reduction and dye oxidation in a TiO_2 slurry reactor, J. Photochem. Photobiol. A: Chem. 147 (2002) 71–76.
[11] Z. Sun, L. Zheng, S. Zheng, R.L. Frost, Preparation and characterization of TiO_2/acid leached serpentinite tailings composites and their photocatalytic reduction of chromium(VI), J. Colloid Interface Sci. 404 (2013) 102–109.
[12] H. Ichiura, T. Kitaoka, H. Tanaka, Removal of indoor pollutants under UV irradiation by a composite TiO_2-zeolite sheet prepared using a papermaking technique, Chemosphere 50 (2003) 79–83.
[13] J. Castañeda-Contreras, V.F. Marañón-Ruiz, R. Chiu-Zárate, H. Pérez-Ladrón de Guevara, R. Rodriguez, C. Michel-Uribe, Photocatalytic activity of erbium-doped TiO_2 nanoparticles immobilized in macro-porous silica films, Mater. Res. Bull. 47 (2012) 290–295.
[14] K. Saeki, M. Kadono, A. Nabeshima, Removal of aqueous chromate [Cr (VI)] through photocatalysis by using TiO_2-coated silica granules, J. Environ. Sci. Health A: Toxic/Hazard. Subst. Environ. Eng. 45 (2010) 275–281.
[15] M.A.M. Khraisheh, Y.S. Al-degs, W.A.M. McMinn, Remediation of wastewater containing heavy metals using raw and modified diatomite, Chem. Eng. J. 99 (2004) 177–184.
[16] P. Yuan, D. Liu, M. Fan, D. Yang, R. Zhu, F. Ge, J. Zhu, H. He, Removal of hexavalent chromium [Cr (VI)] from aqueous solutions by the diatomite-supported/unsupported magnetite nanoparticles, J. Hazard. Mater. 173 (2010) 614–621.
[17] S. Sungworawongpana, S. Pengprecha, Calcination effect of diatomite to chromate adsorption, Proc. Eng. 8 (2011) 53–57.
[18] Y. Liu, S. Zheng, G. Du, F. Shu, J. Chen, Photocatalytic degradation property of nano-TiO_2/diatomiate for Rodamine B dye wastewater, Int. J. Mod. Phys. B 23 (2009) 1683–1688.
[19] N. Wang, Y. Xu, L. Zhu, X. Shen, H. Tang, Reconsideration to the deactivation of TiO_2 catalyst during simultaneous photocatalytic reduction of Cr(VI) and oxidation of salicylic acid, J. Photochem. Photobiol. A: Chem. 201 (2009) 121–127.
[20] X. Wang, S.O. Pehkonen, A.K. Ray, Removal of aqueous Cr(VI) by a combination of photocatalytic reduction and coprecipitation, Ind. Eng. Chem. Res. 43 (2004) 1665–1672.
[21] G. Cappelletti, C.L. Bianchi, S. Ardizzone, Nano-titania assisted photoreduction of Cr(VI): the role of the different TiO_2 polymorphs, Appl. Catal. B: Environ. 78 (2008) 193–201.
[22] L. Yang, Y. Xiao, S. Liu, Y. Li, Q. Cai, S. Luo, G. Zeng, Photocatalytic reduction of Cr(VI) on WO_3 doped long TiO_2 nanotube arrays in the presence of citric acid, Appl. Catal. B: Environ. 94 (2010) 142–149.
[23] L.B. Khalil, W.E. Mourad, M.W. Rophael, Photocatalytic reduction of environmental pollutant Cr(VI) over some semiconductors under UV/visible light illumination, Appl. Catal. B: Environ. 17 (1998) 267–273.
[24] K. Kabra, R. Chaudhary, R.L. Sawhney, Solar photocatalytic removal of metal ions from industrial wastewater, Environ. Prog. 27 (2008) 487–495.
[25] R. Qiu, D. Zhang, Z. Diao, X. Huang, C. He, J.L. Morel, Y. Xiong, Visible light induced photocatalytic reduction of Cr (VI) over polymer-sensitized TiO_2 and its synergism with phenol oxidation, Water Res. 46 (2012) 2299–2306.
[26] C. Tian, S. Huang, Y. Yang, Anatase TiO_2 white pigment production from unenriched industrial titanyl sulfate solution via short sulfate process, Dyes Pigments 96 (2013) 609–613.
[27] Q. Zhang, L. Gao, J. Guo, Effects of calcination on the photocatalytic properties of nanosized TiO_2 powders prepared by $TiCl_4$ hydrolysis, Appl. Catal. B: Environ. 26 (2000) 207–215.
[28] K. Tanaka, M.F.V. Capule, T. Hisanaga, Effect of crystallinity of TiO_2 on its photocatalytic action, Chem. Phys. Lett. 187 (1991) 73–76.
[29] H.S. Lee, S.M. Koo, J.W. Yoo, TiO_2–SiO_2 nanoparticles for suppressing photocatalytic activities and improving hydrophilicity, J. Ceram. Process. Res. 13 (2013) s300–s303.
[30] Z. Sun, Z. Bai, H. Shen, S. Zheng, R.L. Frost, Electrical property and characterization of nano-SnO_2/wollastonite composite materials, Mater. Res. Bull. 48 (2013) 1013–1019.
[31] R. Chen, H. Liu, Preparation of Cr-doped TiO_2/SiO_2 photocatalysts and their photocatalytic properties, J. Chin. Chem. Soc. 58 (2011) 947–954.
[32] C.H. Kim, B.H. Kim, K.S. Yang, TiO_2 nanoparticles loaded on graphene/carbon composite nanofibers by electrospinning for increased photocatalysis, Carbon 50 (2012) 2472–2481.
[33] H. Fu, G. Lu, S. Li, Kinetic and mechanism study on photocatalytic detoxification of Cr (VI) ions on TiO_2 catalyst, Toxicol. Environ. Chem. 70 (1999) 333–347.
[34] J.K. Yang, S.M. Lee, M. Farrokhi, O. Giahi, M. Shirzad Siboni, Photocatalytic removal of Cr (VI) with illuminated TiO_2, Desalination Water Treat. 46 (2012) 375–380.
[35] V. Pifferi, F. Spadavecchia, G. Cappelletti, E.A. Paoli, C.L. Bianchi, L. Falciola, Electrodeposited nano-titania films for photocatalytic Cr(VI) reduction, Catal. Today 209 (2013) 8–12.
[36] S. Chakrabarti, B. Chaudhuri, S. Bhattacharjee, A.K. Ray, B.K. Dutta, Photoreduction of hexavalent chromium in aqueous solution in the presence of zinc oxide as semiconductor catalyst, Chem. Eng. J. 153 (2009) 86–93.
[37] K.M. Joshi, V.S. Shrivastava, Photocatalytic degradation of Chromium (VI) from wastewater using nanomaterials like TiO_2, ZnO, and CdS, Appl. Nanosci. 1 (2011) 147–155.
[38] C.O.A. Olsson, S.E. Hörnström, An AES and XPS study of the high alloy austenitic stainless steel 254 SMO® tested in a ferric chloride solution, Corros. Sci. 36 (1994) 141–151.
[39] C. Wang, H. Shi, Y. Li, Synthesis and characterization of natural zeolite supported Cr-doped TiO_2 photocatalysts, Appl. Surf. Sci. 258 (2012) 4328–4333.
[40] M. Harju, S. Areva, J.B. Rosenholm, T. Mäntylä, Characterization of water exposed plasma sprayed oxide coating materials using XPS, Appl. Surf. Sci. 254 (2008) 5981–5989.
[41] B. Stypula, J. Stoch, The characterization of passive films on chromium electrodes by XPS, Corros. Sci. 36 (1994) 2159–2167.
[42] W. Cao, Z. Dang, G.-N. Lu, Kinetics and mechanism of Cr (VI) sorption from aqueous solution on a modified lignocellulosic material, Environ. Eng. Sci. 30 (2013) 672–680.
[43] A. Idris, N. Hassan, R. Rashid, A.-F. Ngomsik, Kinetic and regeneration studies of photocatalytic magnetic separable beads for chromium (VI) reduction under sunlight, J. Hazard. Mater. 186 (2011) 629–635.
[44] Q. Yang, Y. Liao, L. Mao, Kinetics of photocatalytic degradation of gaseous organic compounds on modified TiO_2/AC composite photocatalyst, Chin. J. Chem. Eng. 20 (2012) 572–576.
[45] R. Jiang, H.Y. Zhu, G.M. Zeng, L. Xiao, Y.J. Guan, Synergy of adsorption and visible light photocatalysis to decolor methyl orange by activated carbon/nanosized CdS/chitosan composite, J. Central South Univ. Technol. 17 (2010) 1223–1229.
[46] J.P.S. Valente, P.M. Padilha, A.O. Florentino, Studies on the adsorption and kinetics of photodegradation of a model compound for heterogeneous photocatalysis onto TiO_2, Chemosphere 64 (2006) 1128–1133.
[47] I.K. Konstantinou, V.A. Sakkas, T.A. Albanis, Photocatalytic degradation of propachlor in aqueous TiO_2 suspensions. Determination of the reaction pathway and identification of intermediate products by various analytical methods, Water Res. 36 (2002) 2733–2742.